arXiv:cond-mat/0312613v2 [cond-mat.soft] 24 Dec 2003

Precision Feshbach spectroscopy of ultracold Cs_2

Cheng Chin*, Vladan Vuletić†, Andrew J. Kerman‡, Steven Chu
Department of Physics, Stanford University, Stanford, California 94305-4060

Eite Tiesinga, Paul J. Leo§, and Carl J. Williams
Atomic Physics Division, National Institute of Standards and Technology, Gaithersburg, Maryland 20899-8423

We have observed and located more than 60 magnetic field-induced Feshbach resonances in ultracold collisions of ground-state ^{133}Cs atoms. These resonances are associated with molecular states with up to four units of rotational angular momentum, and are detected through variations in the elastic, inelastic, and radiative collision cross sections. These observations allow us to greatly improve upon the interaction potentials between two cesium atoms and to reproduce the positions of most resonances to accuracies better than 0.5%. Based on the relevant coupling scheme between the electron spin, nuclear spin, and orbital angular momenta of the nuclei, quantum numbers and energy structure of the molecular states beneath the dissociation continuum are revealed. Finally, we predict the relevant collision properties for cesium Bose-Einstein condensation experiments.

PACS numbers: 34.50.-s, 05.30.Jp, 32.80.Pj, 67.40.Hf

I. INTRODUCTION

The collision properties of an ultracold and dilute atom gas are strongly influenced by the long-range interactions between two atoms. When the interaction potential supports a weakly bound state near the scattering energy, the atomic collision properties can be resonantly altered, a situation referred to as a Feshbach resonance [1, 2]. In many cold-atom systems, magnetically tunable Feshbach resonances have been discovered, and have led to ground-breaking observations including the implosion of a Bose-Einstein condensate (BEC) [3], the coherent coupling between an atomic BEC and molecules [4], the creation of bright solitons [5], and recently the creation of ultracold molecules [6, 7, 8] and of a molecular BEC [9].

The collisional properties of ultracold cesium atoms have intrigued experimentalists and theorists because of their large clock shifts [10], enormous collision cross sections [11], and extreme difficulty to reach BEC [12]. These anomalies in the atom-atom scattering can be explained by the coupling of the scattering continuum to molecular states. While these states cannot be accessed by conventional spectroscopy [13], they may be tuned into resonance with the scattering continuum and induce Feshbach resonances. Detection of multiple Feshbach resonances, or Feshbach spectroscopy, permits a precise determination of the long-range interaction parameters, as well as the molecular structure near threshold. With this information, the cold collision anomalies can be resolved and the clock shifts [14], collision cross sections and scattering lengths can be accurately calculated [15].

In this work, we report the observation of more than 60 Feshbach resonances of cesium atoms in 10 different incident channels. In particular, we employ a radiative detection scheme to resolve narrow resonances [6, 16] whose locations allow us to significantly improve our determination of Cs interaction parameters over our previous work [15, 17]. With these parameters, the molecular energy structure near threshold, as well as *s*-wave scattering lengths and collision properties can be precisely determined.

We organize the paper as follows. First, we outline the experimental setup and procedures, and the general measurement methods in Sec. II. We present and discuss the results from inelastic Feshbach spectroscopy, elastic Feshbach spectroscopy and radiative spectroscopy in Sections III, IV, and V, respectively. In Section VI we discuss the Hamiltonian for two ground-state cesium atoms and approximate quantum numbers in the system. The numerical procedures for calculating scattering properties and bound state energies are presented in Sec. VII. Section VIII analyses all observed Feshbach resonances and assigns quantum numbers to each resonance.

II. EXPERIMENT

A. Feshbach spectroscopy

Feshbach resonance in binary atomic collisions is illustrated in Fig. 1. Interacting atom pairs in the scattering continuum, or scattering channel, couple to a discrete bound state supported by a closed channel with higher internal energy. This coupling resonantly alters the outgoing scattering amplitude in the scattering channel (elastic collision resonance) and in the lower-lying open channels (inelastic collision resonance).

---

*Present Address: Institut für Experimentalphysik, Universität Innsbruck, Technikerstr. 25, 6020 Innsbruck, Austria
†Present Address: MIT-Harvard Center for Ultracold Atoms, Massachusetts Institute of Technology, Cambridge, MA 02139
‡Present Address: Yale University Physics Department, Sloane Laboratory, 260 Whitney Ave., New Haven, CT 06520
§Present Address: National Human Genome Research Institute, 49 Convent Drive, Bldg 49, Bethesda, MD 20874-4472

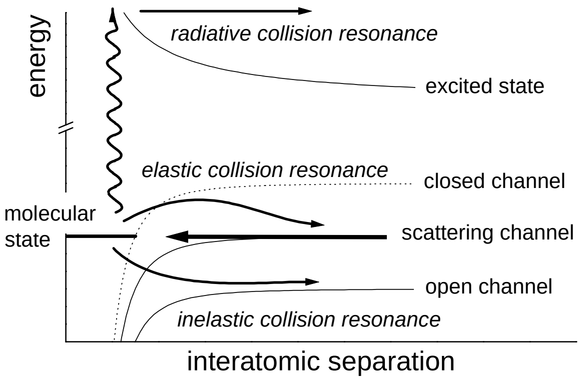

FIG. 1: Illustration of radiative, elastic, and inelastic Feshbach resonance. The molecular state is supported by the closed channel.

In ultracold atom experiments, Feshbach resonances can be observed in elastic and inelastic collision rates [2, 18] and in the molecular population, probed by photoassociation [19], or photodissociation [6] as shown in Fig. 1.

In most cases the magnetic moments of the molecular state and the scattering continuum are unequal, such that the energy difference between the molecular state and the colliding atom pair can be tuned by means of an external magnetic field. The molecular bound-state energy structure near dissociation threshold is then reflected in the magnetic-field dependence of the atom-atom scattering. A measurement of the ultracold collision properties as a function of magnetic field (Feshbach spectrum) in combination with theoretical modeling thus unveils the underlying molecular spectrum. In this work, we are able to associate each resonance with its quantum numbers of both the incoming scattering channel and the molecular state, where it is noteworthy that the s-, p-, d-…partial wave of the incoming channel and of the resonance need not be the same. A collection of Feshbach spectra for colliding atoms in several different quantum states then provides the information necessary to accurately determine the long-range interaction parameters and the molecular energy structure near the dissociation continuum.

B. Preparation of ultracold high-density samples

In order to measure Feshbach spectra with good signal-to-noise ratio and high resolution, and to simplify the theoretical analysis, it is favorable to use high-density samples of ultracold atoms confined in a trap that produces negligible tensor light shifts of the atomic and molecular energy levels [20]. We use a far-detuned, linearly polarized, one-dimensional ($1D$) optical lattice trap to confine the atoms, in conjunction with an optical cooling method that can produce high-density samples at μK temperatures [21, 22].

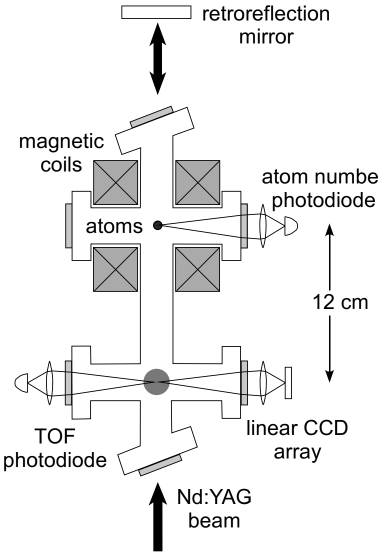

FIG. 2: Apparatus for Feshbach spectroscopy of ^{133}Cs.

Fig. 2 shows schematically the experimental setup. Ultracold samples of cesium atoms are prepared in the upper part of a compact ultrahigh vacuum chamber. A pair of magnetic field coils, when operated in the anti-Helmholtz configuration with opposite currents, provides the spherical quadrupole field for a magneto-optical trap (MOT), and, in the Helmholtz configuration, produces a homogeneous magnetic field up to 25 mT. A linearly polarized, vertically propagating, retroreflected Nd:YAG laser beam provides the far-detuned one-dimensional lattice dipole trap at 1064 nm [21]. The number of trapped atoms is inferred from the fluorescence emitted by the cloud when it is illuminated with resonant light on the $F_g = 4 \rightarrow F_e = 5$ hyperfine component of the D_2 line near 852 nm. Cloud temperatures in the vertical and horizontal directions are determined by releasing the atoms and performing time-of-flight imaging 12 cm below onto a photodiode and a linear CCD array, respectively. Trap vibration frequencies are measured by parametric excitation [23]. The atomic density is derived from the measured atom number, temperature and trap vibration frequencies, as detailed in Ref. [17].

The ultracold sample is prepared by first collecting 5×10^8 atoms in a vapor-cell magneto-optical trap (MOT) in 500 ms. Superimposed with the MOT is the YAG $1D$ optical lattice dipole trap that at a power of 8 W and a beam waist of 260 μm provides a trap depth of $U/h = 1.6$ MHz, and axial and radial vibration frequencies of $\omega_a/2\pi = 50$ kHz and $\omega_r/2\pi = 80$ Hz, respectively. The preparation of the high-density sample in the YAG dipole trap is accomplished by means of two phases of Raman-sideband cooling (RSC) with a $3D$ near-detuned optical lattice [22]. We extinguish the MOT light and apply the first RSC for 10 ms in a small bias field of 5 μT, which cools the atoms to temperatures below 1 μK, and predominantly polarizes them into the lowest-energy magnetic sublevel $|6S_{1/2}, F = 3, m_F = 3\rangle$. Here F is the total angular momentum of cesium atoms in the $6S_{1/2}$ ground state and m_F is the angular momentum projection along the magnetic field direction. When the $3D$ near-detuned optical lattice is extinguished in 1 ms, the release of the atoms into the $1D$ YAG lattice trap is adiabatic only in the vertical direction, and we observe a radial oscillation as the atoms slide down the trap potential. To remove some of the excess potential energy, we wait for 4 ms until the atoms have the greatest kinetic energy and highest density, and perform a second phase of RSC [24]. Due to the high density near 10^{12} cm^{-3}, the second cooling requires a weaker optical pumping intensity and longer cooling time of 15 ms. After rethermalization for 200 ms in the YAG lattice trap, 1×10^8 atoms are prepared at a temperature of 3 μK to 5 μK with a vertical (horizontal) rms radius of $\sigma_z = 580$ μm ($\sigma_x = 30$ μm). This means that near the central region, each site in the 1D YAG lattice trap contains 4×10^4 atoms at a mean density of approximately 1×10^{13}cm^{-3}. The two phases of RSC also allow us to adjust almost independently the atomic density and temperature by changing the detuning of the optical pumping beam during the first and the second RSC phase, respectively.

The preparation of pure samples in desired target states is crucial for cold collision experiments because different internal states can have drastically different collision properties. To improve the atomic polarization over that achieved by the RSC alone, we apply an additional optical pumping pulse for 3 ms during the release from the second RSC phase. This has the advantage that atom-atom collisions are still suppressed due to the $3D$ confinement in the near-detuned optical lattice, which prevents radiative collision loss. Using microwave spectroscopy, we optimize the optical pumping process at a bias field of 14 μT, and prepare up to 98% of the atoms in one of the stretched states $|F, m_F = \pm F\rangle$, and the remaining atoms in the neighboring $|F, m_F = \pm(F-1)\rangle$ state, where F=3 or 4. Feshbach resonances in four scattering states or channels can be thus studied: $(3,3) + (3,3)$, $(3,-3) + (3,-3)$, $(4,4) + (4,4)$ and $(4,-4) + (4,-4)$, where $(F_1, m_{F1}) + (F_2, m_{F2})$ indicates the collision of one atom in the $|F_1, m_{F1}\rangle$ state with one in the $|F_2, m_{F2}\rangle$ state.

We also prepare mixed samples containing atoms in two different internal states by either detuning the optical pumping beam, or by applying an additional microwave pulse to transfer part of the population. Typically, we prepare 90% of the population in a stretched state $|a\rangle$, and 10% in another state $|b\rangle$. After fully characterizing the collision properties of the $(a)+(a)$ channel, the mixed collisions $(a)+(b)$ can be monitored by either identifying resonances growing with the population in $|b\rangle$, or by selectively detecting only the population in $|b\rangle$. The large population ratio of the two states ensures that $(b)+(b)$ collision processes remain insignificant. Mixed scattering channels investigated in this work include $(3,3)+(3,2)$, $(3,3)+(4,4)$, $(3,3)+(4,3)$, $(3,3)+(4,2)$,$(3,-3)+(3,-2)$ and $(4,-4)+(4,-3)$.

The ability to study all these different scattering channels is crucial to provide information on the molecular bound states near the $(F_1 = 3) + (F_2 = 3)$, $(F_1 = 3) + (F_2 = 4)$, and $(F_1 = 4) + (F_2 = 4)$ hyperfine asymptotes. These span roughly h 18 GHz in binding energy. As was shown in Ref. [15], the molecules have different characteristics near the three dissociation limits, which particularly helps determine the strength of the van der Waals interaction.

After the atoms have thermalized in the dipole trap, a uniform magnetic field up to 25 mT is applied. In order to preserve the atomic polarization during the field ramp, we first increase the field from 14 μT to 200 μT in 200 ms, and then to an arbitrary field value in another 100 ms. The magnetic field experienced by the atoms is calibrated to an accuracy of $\delta B < 0.1\mu T$ at low field and $\delta B/B < 10^{-4}$ at high field from the Zeeman splitting between magnetic sublevels, as measured with microwave spectroscopy [17]. Slowly changing stray fields of typically 50 μT and remnant fields from the magnetized vacuum chamber up to 2 μT are carefully cancelled with six independent bias coils in three orthogonal directions to an accuracy of 0.1 μT for the field, and 2 μT/cm for the field gradient. An effective magnetic field due to residual circular polarization of the YAG trapping beam [20] is monitored with microwave spectroscopy, and reduced below 0.05 μT by linearizing the beam polarization. To suppress the effects of field inhomogeneity and atomic density variation between the various YAG 1D lattice sites, we perform measurements only on the center portion of the cloud within $\pm 0.4\sigma_z$, which contains 900 lattice sites with a mean atomic density variation of $< 10\%$.

III. INELASTIC FESHBACH SPECTROSCOPY

Inelastic collisions occur when the initial scattering state couples to open channels with lower internal energy, see Fig. 1. Due to energy conservation, the internal energy difference is converted into relative kinetic energy of the atom pair, and is either on the order of the ground state hyperfine splitting or the Zeeman energy. In both cases, the energy release is generally much larger than our trap depth and therefore results in a loss of the colliding atom pair from the trap. Near a Feshbach resonance, inelastic loss is either enhanced or suppressed due to constructive or destructive interference between the off-resonant scattering amplitude with the on-resonant amplitude. In this work, we observe mostly enhanced inelastic collision processes, and only one prominent suppression at 7.66 mT in the $(3,3)+(4,2)$ incident scattering channel [17].

Experimentally, the inelastic rates are determined by fitting the mean atom density, $\bar{n}$, to $d\bar{n}/dt = -L\bar{n} - K\bar{n}^2$, where L is an one-body loss rate, and K is the desired collision rate coefficient. If we assume that the atoms

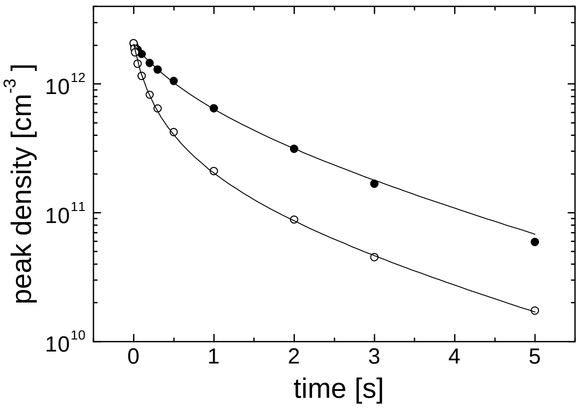

FIG. 3: Resonant and off-resonant time evolution of the atomic density. Atoms are prepared in $|F = 4, m_F = -4\rangle$ at $T = 5.3$ μK and $\bar{n} = 2.1 \times 10^{12}$ cm^{-3} at $B = 14$ μT (solid circles) and $B = 20.53$ mT (open circles), where a strong Feshbach resonance is located. See also Table I.

only reside in the harmonic region of the YAG dipole trap potential and that the cloud is in thermal equilibrium and at constant temperature T during the experiment, then the mean atom density is $\bar{n} = N(m\bar{\omega}^2/4\pi k_B T)^{3/2}$ where N is the atom number in one lattice site, $\bar{\omega} = \omega_z^{1/3}\omega_r^{2/3}$ is the mean vibration frequency, m is the cesium atomic mass, and k_B is the Boltzmann constant. The above differential equation can be solved analytically and directly relates the measured trap loss to the thermally averaged loss coefficient K. The one-body loss rate is the same for all measurements. A typical measurement is shown in Fig. 3 with a holding time up to 5 s.

The loss rates as a function of external magnetic field are measured by observing the atom loss within a holding time between 30 ms to 300 ms, such that the maximum collision loss is less than 30%, and the atomic temperature varies by less than 10%. Slow variations in the initial atom number are monitored after every 10 measurements, and corrected for. On the other hand, to observe and locate weak resonances, we allow the atoms to interact for a longer time up to 500 ms in order to obtain better signal to noise. In this case, we ignore the temperature evolution and report only the fractional loss of atoms.

Collisions between atom pairs in two different internal states, such as $(3,-3)+(3,-2)$, differ from those in the same state in that both the even and odd partial waves can be scattered. In the $(3,-3)+(3,-2)$ channel, for instance, we observe rich Feshbach spectra containing both s- and p-wave resonances.

Positions of the inelastic Feshbach resonances are tabulated in Tables I and II.

A. (4,4)+(4,4) inelastic collisions

The stretched $|4,4\rangle$ state was considered a promising candidate for reaching Bose-Einstein condensation in a magnetic trap before the cesium collision properties were revealed. Large inelastic losses that grow as the temperature is reduced were discovered that prevent the condensation of cesium in this state [25, 26, 27].

We find no resonance structure for a sample polarized in the $|4,4\rangle$ state at 5μK, but a loss rate coefficient increasing slowly from 2×10^{-12} cm^{3}s^{-1} to 3×10^{-12} cm^{3}s^{-1} over the range of $B = 0$ to 25 mT. The absence of resonances in this channel is expected since the scattering channel $(4,4)+(4,4)$ has the highest hyperfine and Zeeman energy of all ground-state hyperfine levels, and consequently Feshbach resonances cannot occur.

B. (4,-4)+(4,-4) and (4,-4)+(4,-3) inelastic collisions

We observe two narrow inelastic Feshbach resonances for collisions between two $|4,-4\rangle$ atoms: a weak one at 10.59 mT and a strong one at 20.50 mT. In addition we have discovered an inelastic resonance in the $(4,-4)+(4,-3)$ channel at 20.66 mT. The resonance field values have a ratio of $1:2:2$ to within 3%. This ratio is not a coincidence, but a result of the molecular bound state structure below the continuum. See Table I. All three resonances are identified as originating from bound states with identical binding energy at zero magnetic field.

C. (3,-3)+(3,-3) and (3,-3)+(3,-2) inelastic collisions

The $|3,-3\rangle$ state can be magnetically trapped and several attempts to reach BEC in this state were thwarted by the large collision loss and negative scattering length at low magnetic field [27]. In this work, we observe multiple inelastic resonances for collisions between two such atoms, as shown in Fig. 4. One resonance at 2.18 mT is not identified, see Table II.

In $(3,-3)+(3,-2)$ collisions, multiple s- and p- wave resonances are found and identified by varying the population in the $|3,-2\rangle$ state, shown in Fig. 5. An alternative method to identify mixed state resonances is based on detecting the population in $|3,-2\rangle$ by microwave transitions on samples with 90% of the population in $|3,-3\rangle$ and $\sim$ 10% in $|3,-2\rangle$. In this case, we observe enhanced loss of the $|3,-2\rangle$ population near inelastic collision resonances in the $(3,-3)+(3,-2)$ channel, and suppressed loss of the $|3,-2\rangle$ population near inelastic collision resonances in the $(3,-3)+(3,-3)$ channel, the latter being due to the reduction in density of $|3,-3\rangle$ atoms. This provides a clear distinction between the two collision processes.

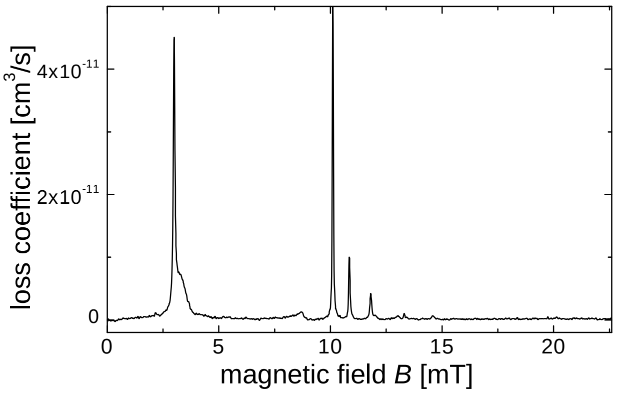

FIG. 4: Binary loss coefficient in a gas of $|F=3, m_F=-3\rangle$ atoms as a function of external magnetic field. The initial mean atomic density is $\bar{n}=5\times10^{12}$ cm^{-3} at a temperature of ~ 5 μK. Populations in the $|F=3, m_F=-3\rangle$, $|F=3, m_F=-2\rangle$ and all other states are 95%, $\sim$ 5% and $<$ 1%, respectively. Magnetic field resolution is 10μT.

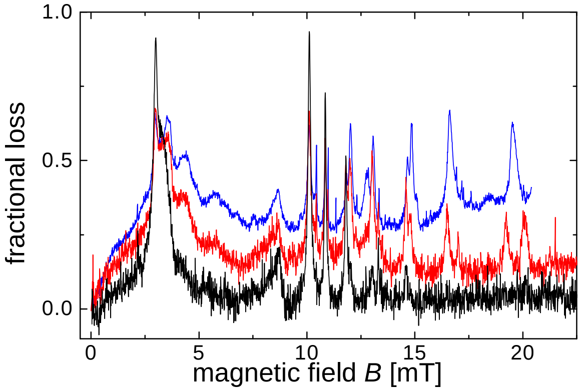

FIG. 5: Atom loss as a function of magnetic field for an initial mean density $\bar{n}=5\times10^{12}$cm^{-3}, temperature of ~ 5 μK and interaction time of 300 ms. Populations in the $|F=3, m_F=-3\rangle$, $|F=3, m_F=-2\rangle$ and all other states are 95%, $\sim$ 5% and $<$ 1% for the lower curve, 85%, $\sim$ 10% and $\sim$ 5% for the middle curve and $\sim$ 70%, $\sim$ 20% and $\sim$ 10% for the upper curve, respectively. Comparison between the curves facilitates the identification of the incident channel responsible for the Feshbach resonances. Magnetic field resolution is 10μT.

D. (3,3)+(3,3) and (3,3)+(3,2) inelastic collisions

The $(3,3)+(3,3)$ channel is the lowest hyperfine scattering channel, and therefore has no binary exothermic collision processes. Collisional inelastic loss is then only due to three-body recombination, a process that falls outside the scope of this paper. A quantitative study of the recombination loss in the $|3,3\rangle$ state is given in Ref. [28]. In collisions between $|3,3\rangle$ and $|3,2\rangle$ atoms we have observed no resonances below B=23.5 mT. Theory predicts weak resonances that are beyond the sensitivity of our current experiment.

E. (3,3)+(4,2), (3,3)+(4,3), and (3,3)+(4,4) inelastic collisions

Multiple Feshbach resonances due to $(3,3)+(4,2)$ and $(3,3)+(4,3)$ scattering are observed in samples with 80% population in $|3,3\rangle$, and 15% in $|4,3\rangle$ or $|4,2\rangle$. The remaining atoms are predominantly in the $|3,2\rangle$ hyperfine state. We have verified that $(3,3)+(3,2)$, $(4,3)+(3,2)$ and $(4,2)+(3,2)$ processes do not contribute to the loss.

We prepare the sample by first polarizing 95% of the atoms in the $|3,3\rangle$ state at $B=14\mu$T, and then apply a microwave pulse for a few ms, which selectively transfers approximately 15% of the population into $|4,3\rangle$ or $|4,2\rangle$. Due to the almost identical energy splitting between the $|3,3\rangle \leftrightarrow |4,2\rangle$ and $|3,2\rangle \leftrightarrow |4,3\rangle$ microwave transitions at low field, we have a small population of $|4,3\rangle$ in the experiment aimed at finding resonances in a $(3,3)+(4,2)$ collision. Pollution by $|3,3\rangle+|4,3\rangle$ resonances occurs, as was previously reported in Ref. [17].

We also observe a weak pollution by $(3,3)+(4,2)$ resonances in the $(3,3)+(4,3)$ spectrum. This cannot be explained by microwave transitions, since $|3,3\rangle \leftrightarrow |4,3\rangle$ and $|3,2\rangle \leftrightarrow |4,2\rangle$ do not have the same frequency. A possible process that creates atoms in the $|4,2\rangle$ state is the inelastic collision process $(3,2)+(4,3)\rightarrow(3,3)+(4,2)$. At low fields the hyperfine and Zeeman energy difference between the final and initial state is $\delta E = k_B 0.52\mu$K $\times(B/mT)$. For our atomic temperatures and magnetic fields, this endothermal spin-changing collisions can create atoms in the $|4,2\rangle$ state.

The four resonances in the $(3,3)+(4,2)$ channel at 6.17 mT, 8.38 mT, 11.0 mT and 11.2 mT, and all four resonances observed in the $(3,3)+(4,3)$ channel at 12.9 mT, 17.3 mT, 22.7 mT and 23.0 mT are paired with identical ratio of the field values 2.07(2). This observation is confirmed by the theoretical identification of the paired resonances as being due to molecular states with identical binding energy at zero magnetic field.

In a separate experiment we have found no inelastic resonances in $(3,3)+(4,4)$ collisions for magnetic field strengths up to 23.5 mT, in agreement with theory.

IV. ELASTIC FESHBACH SPECTROSCOPY

The resonant change of the scattering amplitude in the incident channel also results in a modification of the elastic cross section. We refer to this process as an elastic Feshbach resonance, see Fig. 1. Beside the direct measurement of the thermalization rate between the axial and radial motion [18, 29], we have developed a more sensitive measurement technique for elastic Feshbach resonances, the measurement of the evaporation rate in a shallow trap [17]. This method converts the temperature evolution measurement into an atom number measurement, which provides better sensitivity and signal-to-noise ratio.

We report elastic collision properties in the pure

$(3,3)+(3,3)$ channel and in the mixed $(3,3)+(3,2)$ channel, where the measurements are not complicated by inelastic processes. The elastic spectrum of the $(3,3)+(3,3)$ channel has previously been reported in Refs. [17, 18]. Although the elastic cross section can in principle be both enhanced and decreased by the Feshbach resonance, we observe only dips in the elastic cross section at T=5 μK. This is due to the large background scattering length, resulting in an elastic cross section that is mostly unitarity limited to $\sigma = 8\pi/k^2$ ($\sigma = 4\pi/k^2$) when the colliding cesium atoms are (are not) in the same state. A vanishing elastic collision cross section at 1.7 mT resulting from a strong $s-$wave Feshbach resonance in the $(3,-3)+(3,-3)$ channel was first observed as a reduction in the cross axis thermalization [18]. Three additional $d-$wave Feshbach resonances were observed by monitoring the evaporative loss rate [17]. A vanishing elastic cross section in the $(3,3)+(3,2)$ channel is observed with the same evaporative loss method, where we measure the remaining atom number in $|3,2\rangle$. Positions of the elastic collision rate minima are given in Table I.

The elastic collision measurements based on evaporative loss are limited to resonances whose width in energy is comparable to or exceeds the thermal energy of the sample k_BT. For narrow resonances the resonant variation of the elastic collision rate over a small interval of collision energies does not lead to observable variations in the evaporation rate. For the detection of such weak resonances we have to resort to radiative Feshbach spectroscopy, discussed in the next section.

V. RADIATIVE FESHBACH SPECTROSCOPY

Narrow resonances with a linewidth that is small compared to the thermal energy k_BT do not significantly affect the sample's thermalization rate, and therefore cannot be probed by elastic Feshbach spectroscopy. However, it is possible to directly measure the enhanced (quasi-)bound state population on a Feshbach resonance using a far-detuned laser beam to selectively dissociate the molecules, while leaving the atoms unperturbed. This technique is called radiative Feshbach spectroscopy. [6, 16].

In this work, we apply radiative Feshbach spectroscopy to probe Feshbach resonances in the $(3,3)+(3,3)$ and $(3,3)+(3,2)$ scattering channels using a probe beam typically detuned 20 GHz to 4 THz to the blue of the cesium D_2 transition at 852.3 nm. The probe beam is provided by a titanium-sapphire laser, and uniformly illuminates the atom sample with a stabilized intensity up to 50W/cm^2. The intensity and detuning of the laser are adjusted such that the single-atom excitation is sufficiently weak, and negligible atom loss is observed when the magnetic field is tuned off the Feshbach resonances, while maximizing the loss on the Feshbach resonance.

To measure the radiative collision loss, we first prepare atom samples either fully polarized in the $|3,3\rangle$ to study $(3,3)+(3,3)$ collisions, or 85% in $|3,3\rangle$ and 15% in $|3,2\rangle$ to study $(3,3)+(3,2)$ collisions. After the preparation and field ramping, we typically illuminate the atoms with the probe beam for t=100 ms to 300 ms, and measure the trap loss. To determine the radiative loss rate as a function of magnetic field, we perform two consecutive atom number measurements at every magnetic field value $B=B_i$ to discriminate non-radiative loss: N_1 is the atom number at $B=B_i$ without the probe beam, and N_2 is obtained at $B=B_i$ with the probe beam. The radiative loss rate is then given by $\gamma = (1-N_2/N_1)/t$, where the illumination time t is chosen to keep the maximum atomic loss below 30%. To increase detection sensitivity on weak resonances, we lengthen t to $>$ 500ms, and average each data point up to 5 times. A detailed spectrum thus obtained is shown in Fig. 6. The details of the radiative loss line shape are discussed in Ref. [16]; atom-molecule dynamics and the sensitivity of the our radiative Feshbach spectroscopy are studied in Ref. [6]. Positions of the resonances are tabulated in Table III. One of the Feshbach resonances observed by radiative Feshbach spectroscopy was recently used to create ultracold cesium molecules [7].

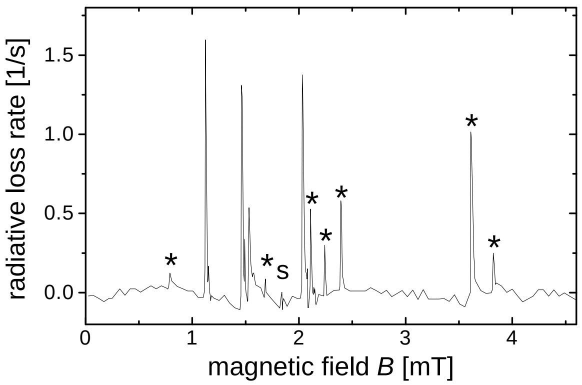

FIG. 6: A detailed radiative loss spectrum with a field resolution of 0.5μT. The probe beam at wavelength $\lambda = 844$ nm has an intensity of 50W/cm^2. 85% (15%) of the atoms are in the $|3,3\rangle$ ($|3,2\rangle$) state. The temperature and mean density of the sample are 3.5μK and 1×10^{13} cm^{-3}, respectively. "S" indicates a shape resonance; the stars indicate Feshbach resonances in the $(3,3)+(3,2)$ channel. Magnetic field resolution near the resonances is 5μT.

VI. THEORY

The structure of the Hamiltonian of two interacting ^2S ground state alkali-metal atoms is well known. It contains the atomic kinetic energy operator, an atomic Hamiltonian for each atom, two Born-Oppenheimer potentials with symmetry $^1\Sigma_g^+$ and $^3\Sigma_u^+$, the nuclear rotation operator $\hbar^2\vec{l}^2/(2\mu R^2)$, and weaker relativistic spin-spin dipole and second order spin-orbit interactions. Here $\vec{l}$ is the nuclear mechanical angular momentum and μ is the reduced mass of the molecule.

The atomic Hamiltonian contains a Fermi contact term and the Zeeman interaction when an external magnetic field, B, directed along the z axis is present during the collision. The eigenstates of the $B = 0$ atomic Hamiltonian are $|F_\alpha, m_{F\alpha}\rangle$, where $\alpha = 1$ or 2 for atom 1 or 2, $\vec{F}_\alpha = \vec{s}_\alpha + \vec{i}_\alpha$ and $m_{F\alpha}$ is the projection of $\vec{F}_\alpha$ along the z axis. Here $\vec{s}_\alpha$ and $\vec{i}_\alpha$ are the atomic electron and nuclear spin, respectively. For $B > 0$, states with the *same* $m_{F\alpha}$ mix, F_α is no longer a good quantum number, and the zero field $m_{F\alpha}$ degeneracy is lifted. For convenience, atomic eigenstates in a magnetic field will be labeled by $|F_\alpha, m_{F\alpha}\rangle$ since for fields used in this paper the Zeeman interaction is small compared to the hyperfine interaction and F_α is an approximately good quantum number. We use hyperfine constants and magnetic moments from Ref. [30]. The nuclear spin of cesium is 7/2.

The selection rules for the Born-Oppenheimer Hamiltonian conserve $\vec{l}$ and $\vec{f} = \vec{F}_1 + \vec{F}_2$. Consequently, bound states and scattering amplitudes can be labeled by fl for $B = 0$ and $m_f l$ for $B > 0$. Here, $m_f = m_{F1} + m_{F2}$. The two relativistic interactions weakly mix states with different l and f. Global symmetries ensure that the molecular Hamiltonian, including the relativistic interactions, conserves parity and total angular momentum $\vec{F} = \vec{f} + \vec{l}$ and its projection $M = m_f + m_l$ for $B = 0$ or only M for nonzero fields. Only even or odd partial waves are coupled. For $B = 0$ there are at most 72 coupled channels while for non-zero field there are infinitely many coupled channels. In practice the number of channels is restricted by using knowledge about the relative strengths of the individual terms in the Hamiltonian.

The relativistic interactions, even though weak, are crucial in understanding the presence of g-wave Feshbach resonances in our gas of ultra-cold Cs atoms. The temperature $T \approx 5$ μK is small compared to the 200 μK and 1 mK barrier height of the d- and g-partial waves, respectively, and only incoming s-wave collisions contribute to the experimental signal. Consequently, coupling from s- to d- and g-waves and back to s-waves is necessary. Small corrections to the location of the Feshbach resonances due to relativistic interactions can be observed.

VII. NUMERICAL APPROACHES

The scattering properties and bound-state energies of the ground state Hamiltonian are obtained with two separate numerical approaches. For scattering the wavefunction at energy E is found using a Gordon propagator[31]. From the scattering wavefunctions elastic and inelastic rate coefficients as a function of magnetic field can be evaluated. Feshbach resonances appear as sharp peaks or dips in the magnetic field dependence of the rate coefficients. For comparison with the experiments the rate coefficients need to be thermally averaged.

Obtaining discrete bound states with the Gordon method is cumbersome since eigenenergies are not *a priori* known and multi-channel scattering wavefunctions need to be calculated at a large number of energies E. Consequently, a discrete variable representation [32] for the radial kinetic energy operator is used to find the bound states. In this approach the eigenvalues of a linear system of size given by the number of radial collocation points times the number of coupled channels need to be calculated. This can be done with standard linear algebra packages. However, resource limitations tend to restrict the number of coupled channels that can be conveniently handled. For the heavy cesium dimer a realistic maximum number of channels lies between 10 to 15, although 20 channels can still be treated. An interesting alternative for finding bound state energies, which does not require the storage of the linear system, can be based on the multi-channel quantum defect theory [33]. It takes advantage of analytic properties of wavefunctions as a function of energy E in order to limit the number of wavefunction evaluations.

Bound states are calculated over a range of magnetic field values. Feshbach resonances occur when a bound state crosses a collisional threshold. Examples of resonances can be found in Refs. [34, 35]. In the absence of the two relativistic interactions calculations label individual bound state by m_f, l, and M. In addition, the field dependence of a level can be traced to a bound state at zero field. At zero field f labels the bound states. For magnetic fields used in our experiment f remains approximately good. Coupling of states with different m_f but the same l are sometimes needed to fully assign the Feshbach resonances. For this paper bound state calculations are used to assign quantum numbers to the resonances.

The Feshbach resonances are experimentally observed in either elastic cross sections, inelastic rate coefficients, or radiative collision rates. The former two measurements can be modeled from first-principle scattering calculations of cross sections and rate coefficients. In principle the rate coefficients need to be thermally averaged. However, a proper thermalization was impractical and for a comparison between theory and experiment only a single collision energy given by the mean collision energy of a gas at temperature T was used. A combination of narrow Feshbach resonances and the need to study the effect of variations in the shape of the two Born-Oppenheimer potentials on the resonance locations would lead to an untenable number of scattering calculations. A one-standard-deviation uncertainty of 0.02 mT to 0.05 mT in the calculated magnetic-field location of the Feshbach resonances observed in elastic or inelastic rates results from the use of a single collision energy.

The radiative collision data require modeling of the rate coefficient for the absorptions of a photon by a pair of ultra-cold Cs atoms [36]. However, we are interested in reproducing the location of Feshbach resonances, and not in the absolute absorption rates. Consequently, from a theoretical perspective it is sufficient to locate the resonances in the elastic cross section in the absence of light. The $l = 4$ (g-wave) resonances observed by radiative Feshbach spectroscopy could not be observed by direct measurement of the elastic cross section.

The energy widths of $l = 4$ (g-wave) Feshbach resonances are significantly smaller than the average collision energy. As a consequence, the location of the maximum of the photoassociation lineshape as a function of magnetic field depends on the zero-collision-energy resonance field location B_0, the temperature, and the magnetic moment $\mu_{\rm res}$ of the embedded bound state. In practice, however, we located the resonances from scattering calculations at $E/k_B = 5.3$ μK and used the magnetic moment of the g-wave Feshbach resonance obtained from bound-state calculations to extrapolate to zero collision energy.

VIII. RESULTS

Tables I, II, and III give the magnetic field locations and assignments of the observed Feshbach resonances. Numbers in parentheses indicate the one standard deviation uncertainty. The locations of the resonances are obtained from elastic and inelastic cross-section measurements or radiative spectroscopy. The theoretical resonance locations are obtained from coupled-channel scattering calculations at a E/k_B=5.3 μK collision energy and Born-Oppenheimer potentials with dispersion coefficients C_6=6890 $E_h a_0^6$ and C_8=954600 $E_h a_0^8$, and scattering lengths $a_S = 280.3$ a_0 and $a_T = 2405$ a_0 [15]. Here k_B is the Boltzmann constant, $1\,E_h = 4.35974$ aJ is a Hartree, and $1\,a_0 = 0.0529177$ nm is a Bohr. $k_B 5.3$ μK is the average collision energy for a Cs gas at T=3.5 μK. For resonances observed in the elastic (inelastic) rates the minimum (maximum) of the line is quoted. The only exception is the resonance at 7.66 mT, where the position of the minimum inelastic rate is given. For the resonances observed by the radiative spectroscopy the maximum of the loss rate and the maximum of the theoretical inelastic collision rate in the absence of laser light are presented.

It should be noted that the magnetic field values for the spectral features presented here should not be confused with the location of the molecular Feshbach state introduced in Fig. 1. Typically, the molecular state can be defined anywhere within the width of the resonance.

The theoretical uncertainties are a consequence of our limited ability to model the experiments, and are obtained by combining the uncertainties due to the spread in collision energies of a thermal Cs gas with the magnetic field dependence of the Feshbach resonance. Any discrepancy between theory and experiment in the tables that lies outside the error bars indicate deficiencies in the shape of the two Born-Oppenheimer potentials.

The assignment of the resonances is obtained by combining information from scattering and bound state calculations. The initial collision partners that lead to a resonance are determined from theoretical scattering calculations, and experimentally by varying the relative population of hyperfine states in the Cs gas and comparing the relative strength of the resonances. The incoming par-

TABLE I: Location and assignment of the observed Feshbach resonances. The first three columns define and give the results of the experiment, where the first column denotes the initial collision state, the second column indicates elastic (el.), inelastic (inel.), or radiative (rad.) measurements, and the third column is the experimental resonance location B_{exp}. The next four columns describe the quantum labels of the resonances. These are the partial wave of the initial collision state, the partial wave of the Feshbach state, the molecular spin f, and its projection m obtained from multichannel *bound state* calculations. The last column gives the theoretical resonance location B_{th} obtained from a multichannel *scattering* calculation at a collision energy of E/k_B=5.3 μK. The resonance at $B_{ex} = 20.66$ mT was not observed in the theoretical scattering calculation due to its extreme narrowness but nevertheless could be assigned from bound state calculations. Several Feshbach resonances have ambiguous assignments (see Text).

	Experiment		Theory				
State	Method	B_{ex}(mT)	Inc. Wave	Assignment l	f	m_f	B_{th}(mT)
(3,3)+(3,3)	el.	$^{\gamma}$1.706(3)	s	s	6	6	1.70(2)
(3,3)+(3,3)	el.	$^{\gamma}$4.802(3)	s	d	4	4	4.79(2)
(3,3)+(3,2)	el.	$^{\gamma}$5.69(2)	s	d	4	4	5.70(2)
(4,-4)+(4,-4)	inel.	10.590(3)	s	d	8	-6	10.58(2)
(4,-4)+(4,-4)	inel.	20.503(3)	s	d	8	-7	20.49(2)
(4,-4)+(4,-3)	inel.	20.66(1)	s	d	8	-6	.
(3,-3)+(3,-3)	inel.	3.005(5)	s	d	6	≈-6	2.99(2)
(3,-3)+(3,-3)	inel.	3.305(5)	s	d	6	-4	3.28(2)
(3,-3)+(3,-3)	inel.	8.69(2)	s	d	8	-8	$^{\beta}$8.80(2)
(3,-3)+(3,-3)	inel.	10.11(2)	s	d	8	-7	10.15(2)
(3,-3)+(3,-3)	inel.	10.88(2)	s	d	8	-6	10.90(2)
(3,-3)+(3,-3)	inel.	11.81(2)	s	d	8	-5	11.85(2)
(3,-3)+(3,-3)	inel.	13.31(2)	s	d	8	-4	13.35(2)
(3,3)+(4,2)	inel.	6.17(2)	s	d	7	5	6.21(2)
(3,3)+(4,2)	inel.	$^{\delta}$7.66(2)	s	s	6	5	7.53(2)
(3,3)+(4,2)	inel.	8.05(2)	p	p	6	5	8.08(2)
(3,3)+(4,2)	inel.	8.38(2)	s	d	7	6	8.43(2)
(3,3)+(4,2)	inel.	11.00(3)	s	d	7	5,7	11.02(2)
(3,3)+(4,2)	inel.	11.20(3)	s	d	7	5,7	11.20(2)
(3,3)+(4,2)	inel.	16.22(4)	s	s	5	5	16.23(2)
(3,3)+(4,2)	inel.	18.29(5)	p	p	5	5	18.45(2)
(3,3)+(4,3)	inel.	12.90(3)	s	d	7	6	12.96(2)
(3,3)+(4,3)	inel.	17.30(4)	p	p	6	6	17.45(2)
(3,3)+(4,3)	inel.	22.73(5)	s	d	7	5,7	22.75(2)
(3,3)+(4,3)	inel.	23.05(5)	s	d	7	5,7	23.13(2)

$^{\beta}$ Temperature-dependent resonance occurred at $Re(a) = 0$.

$^{\gamma}$ Minimum evaporation rate.

$^{\delta}$ Minimum inelastic loss.

TABLE II: Feshbach resonances between two $F = 3$ atoms observed in measurements of inelastic rate coefficients. Columns defined as in Table I. One bound state could not be assigned while three resonances have not been observed experimentally.

	Experiment		Theory				
State	Method	B_{ex}(mT)	Inc. Wave	Assignment l	f	m_f	B_{th}(mT)
(3,-3)+(3,-3)	inel.	2.18(2)					*.
(3,-3)+(3,-2)	inel.	3.57(2)	s	d	6	-5	3.55(5)
(3,-3)+(3,-2)	inel.	10.50(1)	p	f	7	-7	10.50(5)
(3,-3)+(3,-2)	inel.	11.04(2)	p	f	7	-7	11.03(5)
(3,-3)+(3,-2)	inel.	11.39(2)	p	f	7	-7	11.35(5)
(3,-3)+(3,-2)	inel.	12.01(2)	s	d	8	-7	12.03(5)
(3,-3)+(3,-2)	inel.	13.01(2)	s	d	8	-6	13.05(5)
(3,-3)+(3,-2)	inel.	14.58(2)	s	d	8	-5	14.65(5)
(3,-3)+(3,-2)	inel.	17.02(2)	s	d	8	-4	17.05(5)
(3,-3)+(3,-2)	inel.		s	d	8	-3	$^{?}$20.88(5)
(3,-2)+(3,-2)	inel.	$^{\tau}$14.82(2)	s	d	8	-7	14.80(5)
(3,-2)+(3,-2)	inel.	$^{\tau}$16.58(2)	s	d	8	-6	16.50(5)
(3,-2)+(3,-2)	inel.	$^{\tau}$19.25(2)	s	d	8	-5	19.25(5)
(3,-2)+(3,-2)	inel.		s	d	8	-4	$^{?}$23.75(5)
(3,-3+3,-1)	inel.	12.92(2)	s	d	8	-8	12.90(5)
(3,-3+3,-1)	inel.		s	d	8	-4	$^{?}$21.15(5)

* not predicted by calculation.

$^{?}$ not observed experimentally.

$^{\tau}$ has equal contribution from (3,-3)+(3,-1) collision.

TABLE III: Feshbach resonances and a single shape resonance observed with radiative spectroscopy. Columns defined as in Table I. Several Feshbach resonances have ambiguous assignments (see Text).

	Experiment		Theory				
State	Method	B_{ex}(mT)	Inc. Wave	Assignment l	f	m_f	B_{th}(mT)
(3,3)+(3,3)	rad.	1.102(3)	s	g	4	2	1.12(2)
(3,3)+(3,3)	rad.	1.437(3)	s	g	4	3	1.46(2)
(3,3)+(3,3)	rad.	1.506(3)	s	g	6	5	1.51(2)
(3,3)+(3,3)	rad.	1.83(1)	s	d			$^{\epsilon}$1.86(2)
(3,3)+(3,3)	rad.	1.990(3)	s	g	4	4	2.01(2)
(3,3)+(3,3)	rad.	4.797(3)	s	d	4	4	4.77(2)
(3,3)+(3,3)	rad.	5.350(3)	s	g	2	2	5.43(2)
(3,3)+(3,3)	rad.	11.278(3)	s	d	6	4	11.32(2)
(3,3)+(3,3)	rad.	13.106(3)	s	d	4	4	13.19(2)
(3,3)+(3,2)	rad.	0.78(1)	s	g	6	3	0.83(2)
(3,3)+(3,2)	rad.	1.13(1)	s	g	4	1	1.17(2)
(3,3)+(3,2)	rad.	1.47(1)	s	g	4 2 or 6 4		1.54(2)
(3,3)+(3,2)	rad.	1.66(1)	p	f	3	2	1.64(2)
(3,3)+(3,2)	rad.	2.09(1)	s	g	4	3	2.16(2)
(3,3)+(3,2)	rad.	2.21(1)	p	f	1 1 or 3 3		2.18(2)
(3,3)+(3,2)	rad.	2.36(1)	p	f	1 1 or 3 3		2.33(2)
(3,3)+(3,2)	rad.	3.60(1)	s	g	4	4	3.70(2)
(3,3)+(3,2)	rad.	3.81(1)	p	f	5	1	3.78(2)
(3,3)+(3,2)	rad.	4.68(1)	p	f	5	2 or p f=5	4.70(2)
(3,3)+(3,2)	rad.	4.93(1)	p	f	5	2 or p f=5	4.89(2)
(3,3)+(3,2)	rad.	4.99(1)	p	f	5	2 or p f=5	4.99(2)
(3,3)+(3,2)	rad.	5.70(1)	s	d	4	4	5.70(2)
(3,3)+(3,2)	rad.	5.77(1)	p	p	5	3,4,5	5.78(2)
(3,3)+(3,2)	rad.	5.87(1)	p	p	5	3,4,5	5.86(2)
(3,3)+(3,2)	rad.	5.97(1)	p	p	5	3,4,5	5.98(2)

$^{\epsilon}$ *d*-wave shape resonance

tial wave is obtained from scattering calculations. The assignment of quantum numbers l, f, and m_f is made on the basis of bound-state calculations. One resonance could not be assigned.

Levels with the same l,f,m_f symmetry but different $M = m_l + m_f$ are degenerate except for small splittings from the second-order spin-orbit and spin-spin interactions. For even partial waves this is not an issue as losses from the s-wave entrance channel at collision energies of the order of a few microkelvin are much larger than those from d-wave entrance channels and thus only resonances with M equal to the sum of the magnetic quantum number of the initial hyperfine states, $M = m_{fa} + m_{fb}$, are observed. For collisions between atoms in unlike hyperfine states contributions from p-wave collisions cannot be ignored and nearly degenerate Feshbach resonances from three M values appear.

A good example of the complexity for odd l resonances can be found between 4.0 mT and 6.0 mT in the radiative Feshbach spectrum from a $(3, 3) + (3, 2)$ collision. In this region six nearly degenerate resonances are labeled $l = f$, $f = 5$, $m_f = 2$ or $l = p$, $f = 5$. The m_f labels of the p-wave resonance could not be assigned. It turns out that this resonance has a small magnetic moment and at $B \approx$ 5 mT the different m_f components are nearly degenerate. Mixing between different m_f components for the same M due to second-order spin-orbit and spin-spin interactions leads to shifts that are comparable to the spacings due to the Zeeman interaction. The $l = f$ resonances, which have a larger magnetic moment, accidentally reside in the same magnetic field region.

We have assigned more than one set of labels to the resonances between 4.0 mT and 6.0 mT, because m_f and to a lesser degree l and f are not good quantum labels. There are eight different $l = p$, $f = 5$ and $l = f$, $f = 5$, $m_f = 2$ resonances between 4.0 mT and 6.0 mT. Six of these eight resonances are due to the p-wave symmetry. This can easily be checked by noting that only M=4, 5, and 6 can lead to these odd l resonances. Not all eight resonances have been seen which might be due to the fact some are not resolved or unobserved by radiative spectroscopy. We did not perform quantitative *bound*

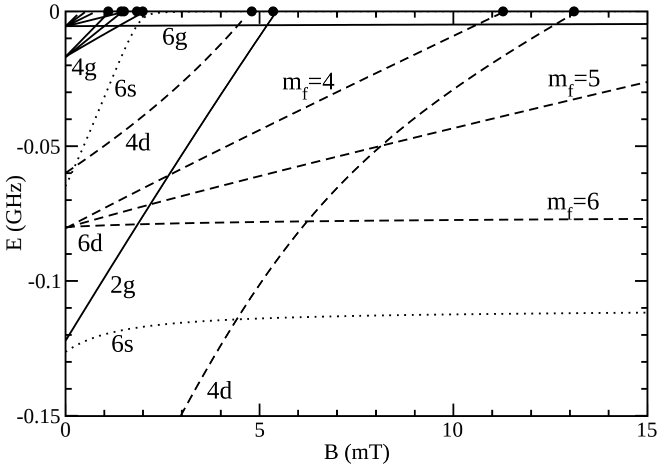

FIG. 7: Total angular momentum projection M=6, s, d, and g-wave bound state energies as a function of magnetic field. The zero of energy corresponds to the $(F = 3, m_F = 3)+(F = 3, m_F = 3)$ dissociation limit. Dotted, dashed, and solid lines correspond to l=s,d, and g states respectively. Furthermore, each curve is labeled by the quantum numbers fl, i.e. $fl = 6s$. The molecular spin f is a zero field quantum number. For the $fl = 6d$ states the magnetic quantum number m_f is also indicated. The filled circles represent the observed threshold resonances.

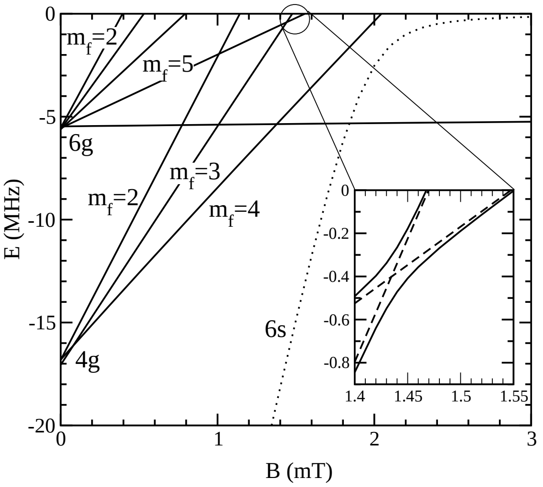

FIG. 8: Expanded view of the M=6, s, d, and g-wave bound states shown in Fig. 7. An avoided crossing between g-wave m_f=3 and 5 bound state occurs around B= 1.4 mT.

state calculations as too many channels must be coupled together. The theoretical field locations listed in the last column of the tables have been obtained from scattering calculations where all states are included at the cost of losing the ability to assign quantum labels.

Fig. 7 shows even l M=6 bound states below the lowest molecular hyperfine state $(3, 3) + (3, 3)$ as a function of magnetic field. Each bound state is labeled with l, f, and m_f. A resonance occurs when a bound state crosses zero energy. The frequency range shown in the figure is sufficient for the assignment of all B <15 mT s, d, and g-wave Feshbach resonances in the collision between $|3, 3\rangle$ Cs atoms. The filled circles mark the observed threshold resonances in a Cs gas at T=3.5 μK ($k_BT/h \sim 0.1$ MHz). Agreement between theory and experiment is sufficiently good that assignments can be made even though discrepancies exist. These discrepancies are caused by the (slightly) incorrect shape of the Born-Oppenheimer potentials and the approximations in the bound state calculations. For fields smaller than 1 mT theory predicts the existence of additional resonances.

The number of coupled channels for M=6 and l=s, d, and g is 74. However, as discussed in the previous section, for nonzero applied magnetic field the coupling between different partial waves and m_f's is due to weak second-order spin-orbit and spin-spin interactions. Consequently, for most resonances in Fig. 7 assignment is unambiguous using independent bound-state calculations that only include states of a given l and m_f. In fact, the curves in the figure have been obtained in this way. However, it should be realized that crossings between bound states shown in the figure are actually avoided when second-order spin-orbit and spin-spin interactions are included. At zero magnetic field coupling between channels with different molecular spin f is also small. The assignment of f is obtained by retracing a bound state to zero magnetic field and noting that $|m_f| \leq f$.

A close look at Fig. 7 shows that the lines can roughly be divided into those that are noticeably curved and those that appear straight. A good example of curved lines are the two $fl = 4d$ bound states, while the $6d$ and $4g$ bound states are good examples of bound states that have a linear magnetic field dependence. The curved lines are due to broad avoided crossings that appear because the same fl labeled states readily mix when a magnetic field is applied. Mixing is due to the interplay of hyperfine, Born-Oppenheimer, and Zeeman interactions and is significantly larger than in avoided crossings mediated by second-order spin-orbit and spin-spin interactions.

The most weakly-bound $fl = 6s$ state is bound by about 65 MHz at zero magnetic field, rises rapidly until it turns over near 2 mT, and then continues just below the dissociation limit. This avoided crossing is also shown in Fig. 8. The bound state does not run parallel to the dissociation limit. It becomes a Feshbach resonance near B=50 mT. The behavior of this bound state has direct consequences for the s-wave scattering length of two $|f_am_a\rangle = |3, 3\rangle$ atoms. Below 1.7 mT the scattering length is negative and above this field value it is positive. This zero of the scattering length has been observed in Ref. [18] and has been used to optimize the Born-Oppenheimer potentials in Refs [15, 17], as well as in this paper. It is interesting to realize that, as discussed in Ref. [15], for B < 1.7 mT d-wave channels affect the elastic scattering and must be included in order to obtain an accurate scattering length.

Some of the M=6 and l=s, d and g Feshbach resonances below B=3 mT could at first not be assigned from

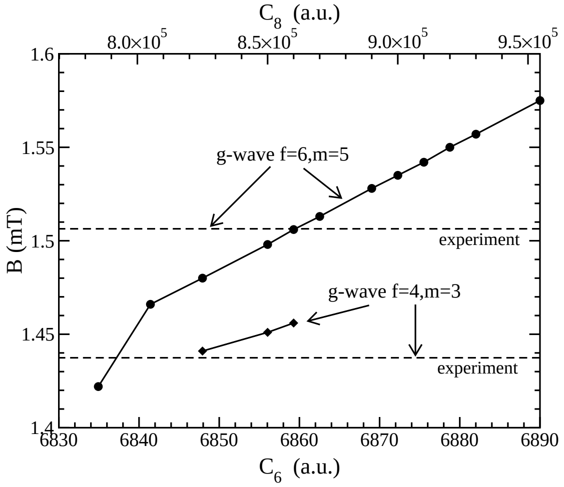

FIG. 9: Position of two $M = 6$ g-wave resonances as a function of C_8 or equivalently C_6 for a zero-energy collision of two Cs atoms in the lowest hyperfine state. The C_6 and C_8 are expressed in units of $E_h a_0^6$ and $E_h a_0^8$, respectively. The dotted lines correspond to the peak of the experimental radiative Feshbach spectroscopy signal.

calculations using states with the same l and m_f. Resonances of different lm_f symmetry lie in the same magnetic field region. Fig. 8 shows a blow up of the 0 mT to 3 mT magnetic field range. The f=4 m_f=3 and f=6 m_f=5 g-wave bound states cross just below the dissociation limit and weak couplings might shift the corresponding Feshbach resonances. The inset shows the avoided crossing between these f=4 m_f=3 and f=6 m_f=5 g-wave bound state when the weak coupling between the two bound states is included. From the figure it is clear that the avoided crossing has little influence on the location of the Feshbach resonances and an fm_f label for each resonance can still be assigned.

The Born-Oppenheimer potentials that have been used for the theoretical resonance locations quoted in Tables I, II, and III and Figs. 7 and 8 are based on the fit in our previous work [15], where the major uncertainties in the calculation of resonance positions arise from the poorly constrained C_8 coefficient. For this Paper we have improved the Born-Oppenheimer potentials by optimizing the C_8 dispersion coefficient in addition to the C_6 coefficient, the strength of the second-order spin-orbit interaction S_C, and the singlet and triplet scattering lengths [15]. For a given C_8 the potentials are optimized to fit the minima in the elastic scattering rate of the $(3,3)+(3,3)$ scattering at 1.7064 mT and 4.8017 mT, the $f = 6$ d-wave resonance in $(3,-3)+(3,-3)$ scattering at 3.0051 mT, and the resonance in $(4,-4)+(4,-4)$ scattering at 20.5029 mT. Over a 10% range of the C_8 coefficient near 900000 $E_h a_0^8$ a linear relationship between C_6, S_C, a_S, and a_T exists.

An improved cesium-dimer Hamiltonian is created by fitting to selected $(3,3)+(3,3)$ g-wave resonances. Fig. 9 shows the M=6, f=6 m_f=5 and f=4 m_f=3, g-wave resonance position as a function of C_8 or equivalently C_6. The figure shows theoretical zero-collision-energy resonance locations derived from E/k_B=5.3 μK calculations and the magnetic moments of the resonances. The peak radiative detection signal as a function of magnetic field is due to collisions at zero energy. The magnetic moment of the resonances is 170 μK/mT for the f=6, m_f=5 and 550 μK/mT for the f=4, m_f=3 state.

The location of the Feshbach resonance found from a bound state calculation, including only g-wave m_f=3 and

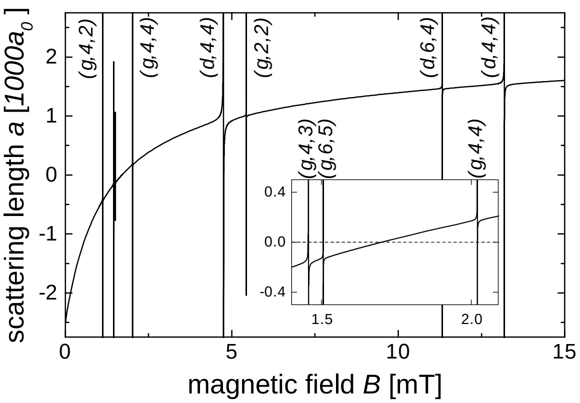

FIG. 10: Scattering length in the $(F = 3, m_F = 3) + (F = 3, m_F = 3)$ scattering channel. Resonances resulted from the M=6, s, d, and g-wave bound states are assigned with quantum number (l, f, m_f), where l is the orbital angular momentum, f is the total internal angular momentum and m_f is the magnetic quantum number. Calculation are done with a magnetic field grid size of 50μT for off-resonance regions and 100nT near the narrow resonances. Inset shows the detail resonance structure near 17G

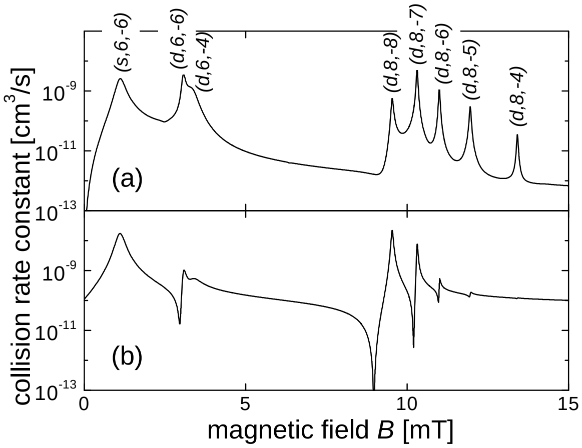

FIG. 11: Collision rate constants in the $(F = 3, m_F = -3) + (F = 3, m_F = -3)$ scattering channel at $E/k_B = 1n$K. Inelastic collision rates (a) and elastic collision rates (b) are calculated with a magnetic field grid size of 10μT for off-resonance regions and 1μT near the resonances. Resonances from the M=-6, s, d, and g-wave bound states are included and assigned with quantum number (l, f, m_f), where the notation is the same as in Fig. 10.

TABLE IV: Properties of the singlet $X^1\Sigma_g^+$ and triplet $a^3\Sigma_u^+$ Born-Oppenheimer potentials and the second-order spin-orbit interaction that give the best fit to all data on collisions between ultra-cold Cs atoms. The C_6 and C_8 are expressed in units of $E_h a_0^6$ and $E_h a_0^8$, respectively. The singlet, a_S, and triplet, a_T, scattering lengths are in units of a_0. S_C is dimensionless. One-standard deviation uncertainties are given.

	value	uncertainty (%)
C_6	6860	0.36
C_8	860 000	8.7
a_S	280.37	0.02
a_T	2440	1.0
S_C	2.6	19

5 channels, and a scattering calculation at zero collision energy, which includes *all* s-, d-, and g-wave channels, disagree by about 0.02 mT. This discrepancy is likely due to the limited number of channels in the bound state calculations. The magnetic moments, however, are not expected to be significantly modified.

Table IV summarizes our best fit. Based on the collision parameters, cold collision properties of cesium atoms can be readily calculated in various scattering channels. In particular, $(3,3)+(3,3)$ and $(3,-3)+(3,-3)$ scattering length is $-2510\ a_0$ at zero magnetic field. In the presence of the magnetic field, Fig. 10 shows the scattering length of the $(3,3)+(3,3)$ channel as a function of magnetic field; Fig. 11 shows the collision rate constants in the $(3,-3)+(3,-3)$ channel at the collision energy of $E = k_B$ 1nK. All s, d, and g wave channels are included in the calculation. These two states are particularly interesting in the experiments of cesium Bose-Einstein condensation [37]. The resonances are identified and labelled by the quantum numbers of the associated molecular states.

IX. CONCLUSION

We have measured > 60 magnetic-field-induced Feshbach resonances in the collision of ultracold ground state cesium atoms. Of all the alkali-metal species cesium is shown to have the richest resonance structure.

The field resonances have been observed in elastic collision rates, evaporation loss rates, collision relaxation rates, as well as in radiative collision resonance experiments (radiative Feshbach spectroscopy). The last experiments have been instrumental in observing $l = 4$ g-wave Feshbach resonances with ∼mG resonance width.

Based on the previous work [15], we have also improved the model for the Cs-Cs collision and in addition used multi-channel bound state calculations to assign each Feshbach resonance with pertinent quantum numbers. The quantum numbers correlate each resonance to a molecular bound state at zero magnetic field. We identify 3 s-wave, 6 $p-$wave, 32 $d-$wave, 10 $f-$wave and 10 $g-$wave Feshbach resonances and one shape resonance. One resonance in the $(3,3)+(3,3)$ channel could not be identified and is possibly a three-body collision resonance or a two-body Feshbach resonance with very high partial-waves number.

The model has been used to calculate the molecular energy structure below the $(F = 3) + (F = 3)$ continuum and the collision properties in the $(3,3)+(3,3)$ and $(3,-3)+(3,-3)$ scattering channels. These data will provide crucial information for experiments on cesium Bose-Einstein condensation [37] and cesium molecules [7].

In general, this paper presents results of a successful collaboration of experimental and theoretical efforts and resolves the collision anomalies of cesium atoms. The excellent agreement on >60 resonances between experiment and theory with only 5 parameters marks a triumph of the predictive power of atomic interaction theory. Since the experimental determination of the resonance locations is better than the theoretical estimate. Further improvements would require more flexibility in the (short-range shape) of the two Born-Oppenheimer potentials. Moreover, theoretical modeling will need to use thermally averaged elastic and inelastic rates as well as an improved model of the radiative lineshape.

X. ACKNOWLEDGEMENT

C.C. would like to thank P.S. Julienne for discussions. This work was supported in part by grants from the AFOSR and the NSF.

[1] E. Tiesinga, B.J. Verhaar, and H.T.C. Stoof, Phys. Rev. A **47**, 4114 (1993)

[2] S. Inouye, M. Andrews, J. Stenger, H.-J. Miesner, S. Stamper-Kurn, and W. Ketterle, Nature **392**, 151 (1998).

[3] E.A. Doney, N.R. Claussen, S.L. Cornish, J.L. Roberts, E.A. Cornell and C.E. Wieman, Nature **412**, 295 (2001).

[4] E.A. Donley, N.R. Claussen, S.T. Thompson, C.E. Wieman, Nature **417**, 529 (2002).

[5] L. Khaykovich, F. Schreck, G. Ferrari, T. Bourdel, J. Cubizolles, L.D. Carr, Y. Castin, and C. Salomon, Science **296**, 1290 (2002); K.E. Strecker, G.B. Partridge, A.G. Truscott, R.G. Hulet, Nature **417**, 150 (2002).

[6] C. Chin, A.J. Kerman, V. Vuletić, S. Chu, Phys. Rev. Lett. **90**, 033201 (2003).

[7] J. Herbig, T. Kraemer, M. Mark, T. Weber, C. Chin, H.-C. Nägerl and R. Grimm, Science **301**, 1510 (2003).

[8] C.A. Regal, C. Ticknor, J.L. Bohn, D.S. Jin, Nature **424**, 47 (2003); K.E. Strecker, G.B. Partridge, R.G. Hulet, Phys. Rev. Lett. **91**, 080406 (2003); J. Cubizolles,T. Bourdel, S.J.J.M.F. Kokkelmans, G.V. Shlyapnikov, C.

Salomon, Phys. Rev. Lett. **91**, 240401 (2003); S. Jochim, M. Bartenstein, A. Altmeyer, G. Hendl, S. Riedl, C. Chin, J. Hecker Denschlag and R. Grimm, Phys. Rev. Lett. **91**, 240402 (2003); K. Xu, T. Mukaiyama, J.R. Abo-Shaeer, J.K. Chin, D. Miller, and W. Ketterle, Phys. Rev. Lett. **91**, 210402 (2003).

[9] S. Jochim, M. Bartenstein, A. Altmeyer, G. Hendl, S. Riedl, C. Chin, J. Hecker Denschlag, and R. Grimm, published online 13 November 2003; 10.1126/science.1093280 (*Science Express*); M. Greiner, C.A. Regal and D.S. Jin, Nature **426**, 537 (2003); M.W. Zwierlein, C.A. Stan, C.H. Schunck, S.M.F. Raupach, S. Gupta, Z. Hadzibabic and W. Ketterle, **91**, 250401 (2003).

[10] K. Gibble and S. Chu, Phys. Rev. Lett. **70**, 1771 (1993).

[11] M. Arndt, M. Ben Fahan, D. Guéry-odelin, M.W. Reynolds, and D. Dalibard, Phys. Rev. Lett. **79**, 625 (1997).

[12] D. Guéry-Odelin, J. Soeding, P. Desbiolles, and Jean Dalibard, Opt. Express **2**, 323 (1998).

[13] H. Weichenmeier, U. Diemer, M. Wahl, M. Raab, W. Wüller, and W. Demtröder, J. Chem. Phys. **82**, 5354 (1985).

[14] P.J. Leo, P.S. Julienne, F.H. Mies, and C.J. Williams, Phys. Rev. Lett. **86**, 3743 (2001).

[15] P.J. Leo, C.J. Williams, P.S. Julienne, Phys. Rev. Lett. **85**, 2721 (2000).

[16] V. Vuletić, C. Chin, A.J. Kerman and S. Chu, Phys. Rev. Lett. **83**, 943 (1999).

[17] C. Chin, V. Vuletić, A.J. Kerman, S. Chu, Phys. Rev. Lett. **85**, 2717 (2000).

[18] V. Vuletić, A.J. Kerman, C. Chin, and S. Chu, Phys. Rev. Lett. **82**, 1406 (1999).

[19] Ph. Courteille, R.S. Freeland, D.J. Heinzen, F.A. van Abeelen and B.J. Verhaar, Phys. Rev. Lett. **81**, 69 (1998).

[20] I.H. Deutsch and P.S. Jessen, Phys. Rev. A **57**, 1972 (1998).

[21] V. Vuletić, C. Chin, A.J. Kerman, and S. Chu, Phys. Rev. Lett. **81**, 5768 (1998).

[22] A.J. Kerman, V. Vuletić, C. Chin, and S. Chu, Phys. Rev. Lett. **84**, 439 (2000).

[23] S. Friebel, C. DAndrea, J. Walz, M. Weitz, and T. W. Hänsch, Phys. Rev. A **57**, R20 (1998).

[24] M.T. DePue, D.J. Han and D.S. Weiss, Phys. Rev. A 63, 023405 (2001).

[25] M. Arndt, M. Ben Fahan, D. Guery-Odelin, M.W. Reynolds, and J. Dalibard, Phys. Rev. Lett. **79**, 625 (1997).

[26] J. Soding, D. Guery-Odelin, P. Desbiolles, G. Ferrari, and J. Dalibard, Phys. Rev. Lett. **80**, 1869 (1998).

[27] D. Guery-Odelin, J. Soding, P. Desbiolles, and J. Dalibard, Opt. Express. **2**, 323 (1998).

[28] T. Weber, J. Herbig, M. Mark, H.-C. Nägerl, and R. Grimm, Phys. Rev. Lett. **91**, 123201 (2003).

[29] J. L. Roberts, N. R. Claussen, James P. Burke, Jr., Chris H. Greene, E. A. Cornell, and C. E. Wieman, Phys. Rev. Lett. **81**, 5109 (1998).

[30] E. Arimondo, M. Inguscio, and P. Violino, Rev. Mod. Phys. **49**, 31 (1977).

[31] R.G. Gordon, J. Chem. Phys. **51**, 14 (1969); R.G. Gordon, Methods Comput. Phys. **10**, 81 (1971).

[32] D.T. Colbert and W.H. Miller, J. Chem. Phys. **96**, 1982 (1992); E. Tiesinga, C.J. Williams, and P.S. Julienne, Phys. Rev. A **57**, 4257 (1998).

[33] M. Raoult and F.H. Mies, Phys. Rev. A **62**, 012708 (2000).

[34] J.M. Vogels, B.J. Verhaar, and R.H. Blok, Phys. Rev. A **57**, 4049 (1998).

[35] T. Laue, E. Tiesinga, C. Samuelis, H. Knöckel, E. Tiemann, Phys. Rev. A, **65**, 023412 (2002).

[36] R. Napolitano, J. Weiner, C. J. Williams, and P. S. Julienne, Phys. Rev. Lett. **73**, 1352 (1994).

[37] T. Weber, J. Herbig, M. Mark, H.-C. Nägerl, R. Grimm, Science **299**, 232 (2003).